Foreign-gas-induced relaxation of Rydberg S and D states in atomic sodium

A. Flusberg,* R. Kachru, T. Mossberg, and S. R. Hartmann
Columbia Radiation Laboratory, Department of Physics, Columbia University, New York, New York 10027
(Received 18 September 1978)

We have measured the He-, Ne-, and Ar-induced relaxation properties of the $3S$-nS ($3S$-nD) superposition states of atomic sodium, where n ranges from 5 to 20 (4 to 34). The measurements were made using the trilevel echo effect. We find that the effective collisional cross section first increases (as a function of n) at low n, and then decreases to a lower asymptotic limit at high n. This behavior is similar to that previously observed for the $3S$-nP series. We also find that the difference between the collisional cross sections for S and D series superpositions closely approximates the inelastic collision cross sections measured elsewhere for the d states. A theoretical description of the trilevel echo effect used to make the measurements is presented.

I. INTRODUCTION

In the early 1930's Füchtbauer and co-workers[1-4] made extensive measurements of foreign-gas-broadened atomic resonance linewidths. This work was remarkable in its scope. The transitions of several alkali metals were studied as a function of foreign-gas pressure for a wide variety of both noble and molecular gases. These studies were carried well into the Rydberg regime. In the case of atomic sodium in an Ar environment the transitions (or more precisely the superposition states) studied ranged from the $3S$-$4P$ all the way up to the $3S$-$25P$. By working over this extended range they made the surprising discovery that while the collisional-broadening cross section increases sharply for increasing principal quantum number n in the low-n region, it quickly reaches a maximum value, and then, as n increases further, it decreases to a small fraction of its maximum value. Above this point it becomes independent of n. There were indications that this limiting cross section is dependent only on the broadening agent and not on the alkali metal whose broadening was studied. Similar measurements have been made more recently by Mazing and Vrublevskaya.[5] Several theoretical treatments of this problem have been presented[6-9] which provide at least a semiquantitative description of this behavior.

Until recently limitations in experimental technique have prevented the study of line broadening from extending beyond the principal series. The development of the Doppler-free two-photon absorption technique,[10,11] however, has made it possible for the first time to study single-photon electric-dipole-forbidden transitions. Biraben *et al.*[12] utilized this technique to measure the sodium $3S$-$4D$ and $3S$-$5S$ collisionally broadened linewidths. By monitoring the decay of two-photon coherent transients as a function of foreign-gas pressure, other workers[13,14] have been able to deduce the foreign-gas-induced broadening of the sodium $3S$-$4D$ superposition state verifying Biraben's results. Experimental difficulties have prevented measurements by these techniques to beyond $n=5$. The development of the trilevel echo effect,[15] however, has made it possible to overcome this impass. As was recently reported[15] the measurement of the trilevel echo intensity versus foreign-gas pressure has made it possible to study the relaxation of several two-photon transitions (two-photon superposition states) in sodium vapor. In this paper we use the trilevel echo effect to study broadening of both the $3S$-nS and $3S$-nD transitions in sodium well into the Rydberg region. Our studies extend over the range $n=5$ to $n=20$ ($n=4$ to $n=34$) for the $3S$-nS ($3S$-nD) transitions.

Aside from extending the range of transitions which can be studied, the trilevel echo technique allows relaxation studies in the presence of low-pressure foreign gases. It is a characteristic of echo experiments that they are relatively unaffected by excitation-pulse spectral widths and by inhomogeneous broadening (Doppler dephasing). This has the advantage of allowing us to make all our measurements at low foreign-gas pressures (<1 Torr), for which only binary collisions should contribute significantly. In contrast, it was necessary for Füchtbauer to raise the foreign-gas pressure to the point at which the pressure broadening exceeded the Doppler width. The high pressure required often modified the linewidth to include an appreciable contribution from multiple collisions, making a simple interpretation of the results difficult.

The availability, by use of the trilevel echo technique, of collision cross sections for S-S superpositions, whose decay represents primarily the

effect of phase-changing (elastic) collisions,[9,16,17] and for S-D superpositions, whose decay represents the combined effect of population transfer[16] (inelastic) and elastic collisions, is potentially quite useful. If one neglects the possibility of interference between the elastic and inelastic contributions to the S-D cross section, it is conceivable that for sufficiently large n^* the inelastic contribution to the S-D cross section can be determined by simply taking the difference between the measured S-D and S-S cross sections. The validity of this conjecture in light of our results will be discussed below.

Before we present our experimental results we define the trilevel technique we use and we obtain formulas for their analysis. This is done in Sec. II. In Sec. III we describe the experimental apparatus. The experimental results are discussed and compared with other experiments and theory in Sec. IV. Appendix A generalizes the theory of Sec. II to an energy-level scheme in which each level consists of several degenerate states, while Appendix B explains what the echo polarization direction should be. Finally, Appendix C describes a second type of trilevel echo which we utilized in a small number of our experiments.

II. THEORY

A. Basic description

The term trilevel echo refers to a class of echo phenomena which has many elements. It is characterized by the sequential excitation of the three energy levels of the individual atoms or molecules of a sample in such a way that a macroscopic oscillating electric-dipole moment involving two of the levels forms at a well-defined time after the last excitation pulse. Only two elements of the trilevel echo class are used in obtaining the data discussed in this paper. This first and most important case involves (a) the excitation of an "ordered superposition of the ground state and an excited state of the same parity via an intermediate state, (b) the subsequent transfer of the ordered superposition to the ground and intermediate states by a later excitation pulse, and (c) the delayed coherent emission (echo) from the ground-intermediate state superposition. Since the data obtained herein is obtained almost exclusively by this kind of technique we devote this section to a careful definition of this element [we call these echoes type-I sum-frequency trilevel echoes (SF-I echoes)] and a weak-excitation-pulse analysis of the effect.

In addition to the SF-I echoes mentioned above we have also used trilevel echoes which differ from the SF-I echoes by the necessity of temporally overlapping the first two excitation pulses.

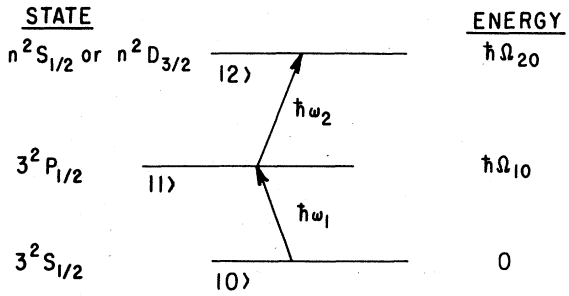

FIG. 1. Schematic of the three levels involved in the production of a trilevel echo. In our experiments the principal quantum number of the upper level $|2\rangle$ ranges from 5 to 20 (4 to 34) when the state is an S (D) state.

These echoes (SF-II echoes) are defined and analyzed in Appendix C.

Consider a dilute gas of identical atoms each of unperturbed atomic Hamiltonian H_0 whose eigenstates $|m\rangle$ satisfy $H_0|m\rangle = \hbar\Omega_m|m\rangle$. We focus our attention on the ground state $|0\rangle$ and two additional discrete electronic eigenstates $|1\rangle$ and $|2\rangle$, such that $\hbar\Omega_0 < \hbar\Omega_1 < \hbar\Omega_2$. (For our experiments in Na, $|0\rangle$ and $|1\rangle$ will correspond to the $3\,^2S_{1/2}$ and $3\,^2P_{1/2}$ states, while $|2\rangle$ will correspond to a higher $n\,^2S_{1/2}$ or $n\,^2D_{3/2}$ state; see Fig. 1.) In the present simplified treatment each electronic state is assumed to be discrete; the optical electric fields and dipole matrix elements p_{ij} between states i and j, are treated as scalars. We generalize in Appendix A to the degenerate case in which $|0\rangle$, $|1\rangle$, and $|2\rangle$ each stand for a manifold of states of equal (or nearly equal) energy. Let $\Omega_{ij} = \Omega_i - \Omega_j$. As shown in Fig. 2(a) the system of atoms is irradiated successively by three light pulses of central frequencies ω_1, ω_2, and ω_3, where $\omega_1 \equiv \Omega_{10}$ and $\omega_2 = \omega_3 \equiv \Omega_{21}$. The central wave vector of the ith pulse is $\vec{k}_i = k_i\hat{n}_i$; we consider only the case $\hat{n}_2 = \hat{n}_3 = -\hat{n}_1$ [Fig. 2(b)].

In the present calculation, in which we wish to obtain only the lowest-order contribution to the echo, we assume that the excitation due to each pulse is *weak* in the sense that the diagonal density matrix elements which were nonzero at the beginning of a pulse are not significantly modified in magnitude by the pulse. In addition, we treat the atomic trajectories classically and the effect of perturbations such as collisions or spontaneous emission phenomenologically. We assume that the atomic trajectories are rectilinear, and, in view of the expected strong state dependence of active atom-perturber collisions, we neglect collisions which produce small changes of velocity. The limitations of this last approximation have been discussed by Berman and Lamb.[18]

The total Hamiltonian H of an atom located at

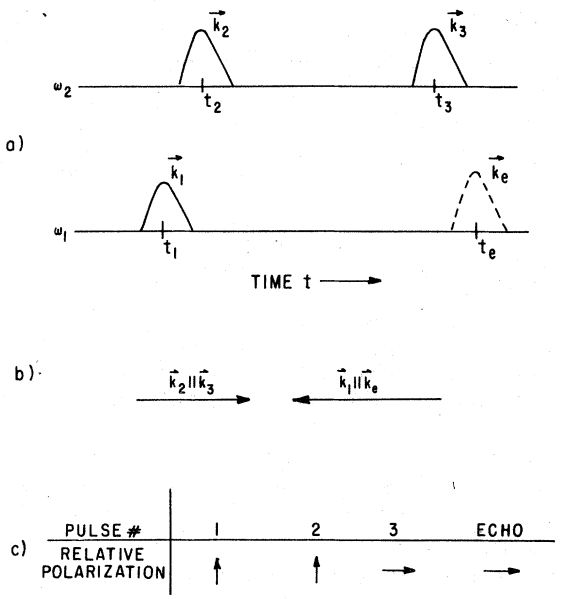

FIG. 2. (a) Temporal sequence of excitation pulses (solid) and echo (dashed) in the case of the SF-I echo. The upper (lower) line shows the pulses at frequency ω_2 (ω_1). The times t_i and wave vectors $\vec{k}_i$ associated with each pulse are shown. (b) Relative propagation directions of excitation pulses and echo. The excitation pulses at frequency ω_2 counterpropagate with respect to the excitation pulse and echo at ω_1. (c) Relative linear polarizations of the three excitation pulses and echo. Note that the echo is polarized perpendicular to the first excitation pulse. This allows us to prevent essentially all potentially obscuring signals from reaching the detector. The second and third excitation pulses propagate antiparallel to the echo and are at frequency ω_2, the first excitation pulse is blocked by a Glan-prism polarizer.

$\vec{X}(t)$ is written

$$H = H_0 - pE(\vec{X}, t) \tag{1}$$

and the density matrix ρ in the Schrödinger picture satisfies

$$\frac{\partial}{\partial t}\rho_{ij} = -\frac{i}{\hbar}[H,\rho]_{ij} - \Gamma_{ij}\rho_{ij} \ . \tag{2}$$

Here Γ_{ij} is the phenomenological relaxation rate of ρ_{ij} which includes decay due to spontaneous emission, collisional dephasing, collisional population transfer out of states i or j, etc. Thus for an initial density matrix in which $\rho_{00} = 1$ and other elements are zero ρ_{10} satisfies

$$\left(\frac{\partial}{\partial t} + i\Omega_{10} + \Gamma_{10}\right)\rho_{10} = \frac{i}{\hbar}(\rho_{00} - \rho_{11})p_{10}E \ . \tag{3}$$

Using $E(\vec{X}, t) = \mathcal{E}_1(\vec{X}, t)e^{i(\vec{k}_1\cdot\vec{X} - \omega_1 t)} + \text{c.c.}$, $\rho_{00} - \rho_{11} \simeq 1$, and the rotating-wave approximation, after the passage of the first pulse we have that

$$\rho_{10}(t) = \rho_{10}^{(1)}(t) = \tfrac{1}{2}i\theta_1 e^{i(\vec{k}_1\cdot\vec{x}_1 - \omega_1 t)}e^{-\Gamma_{10}(t-t_1)} , \tag{4}$$

where

$$\theta_1 = \frac{2p_{10}}{\hbar}\int \mathcal{E}_1(\vec{x}_1, t')e^{i\vec{k}_1\cdot\Delta\vec{x}_1(t')}e^{\Gamma_{10}\Delta t_1}dt' \ . \tag{5}$$

Here $\Delta\vec{X}_i = \vec{X} - \vec{x}_i$ and $\Delta t_i = t' - t_i$, where t_i denotes the central time of the ith excitation pulse and $\vec{x}_i$ is the location of the atom at t_i ($i = 1, 2, 3$). The integration here and for both subsequent pulses is performed over the duration of the pulse. We have assumed that $\mathcal{E}_1(\vec{X}, t') \simeq \mathcal{E}_1(\vec{x}_1, t')$. For an unchirped pulse short enough so that the atom can be considered stationary and relaxation can be neglected, $|\theta_1|$ is simply the "tipping angle" produced by the first pulse on the $0 \to 1$ two-level system, i.e., the pulse "area."

The effect of the second pulse $E_2 = \mathcal{E}_2(\vec{X}, t)e^{i(\vec{k}_2\cdot\vec{X} - \omega_2 t)} + \text{c.c.}$ on ρ_{20} may be calculated in a similar fashion from

$$\left(\frac{\partial}{\partial t} + i\Omega_{20} + \Gamma_{20}\right)\rho_{20} = \frac{i}{\hbar}\rho_{10}p_{21}E_2 \ . \tag{6}$$

Assuming the second pulse to be weak enough so that ρ_{10} may be approximated by $\rho_{10}^{(1)}(t)$ throughout, we find immediately that after pulse 2 passes ρ_{20} is given by

$$\rho_{20}(t) = -\tfrac{1}{4}\theta_1\theta_2 \exp[i(\vec{k}_1\cdot\vec{x}_1 + \vec{k}_2\cdot\vec{x}_2 - \Omega_{20}t)] \times e^{-\Gamma_{20}(t-t_2)}e^{-\Gamma_{10}(t_2-t_1)} . \tag{7}$$

Here

$$\theta_2 = \frac{2p_{21}}{\hbar}\int \mathcal{E}_2(\vec{x}_2, t')e^{i\vec{k}_2\cdot\Delta\vec{x}_2(t')}e^{-(\Gamma_{10}-\Gamma_{20})\Delta t_2}dt' \ . \tag{8}$$

As for the first pulse, in the limit of an unchirped, short pulse, θ_2 approaches the tipping angle produced by pulse 2 on the $1 \to 2$ two-level system.

Finally, the third pulse $E_3 = \mathcal{E}_3(\vec{X}, t)e^{i(\vec{k}_3\cdot\vec{X} - \omega_2 t)} + \text{c.c.}$ modifies ρ_{10} according to

$$\left(\frac{\partial}{\partial t} + i\Omega_{10} + \Gamma_{10}\right)\rho_{10} = \frac{i}{\hbar}p_{12}E_3^*\rho_{20} \ . \tag{9}$$

If we assume ρ_{20} is insignificantly affected by the third pulse, then after pulse 3 passes $\rho_{10}(t) = \rho_{10}^{(1)}(t) + \rho_{10}^{(3)}(t)$, where

$$\rho_{10}^{(3)} = -\tfrac{1}{8}i\theta_1\theta_2\theta_3^* \exp[i(\vec{k}_1\cdot\vec{x}_1 + \vec{k}_2\cdot\vec{x}_2 - \vec{k}_3\cdot\vec{x}_3 - \omega_1 t)] \times e^{-\Gamma_{10}(t-t_3)}e^{-\Gamma_{20}(t_3-t_2)}e^{-\Gamma_{10}(t_2-t_1)} \tag{10}$$

and

$$\theta_3 = \frac{2p_{21}}{\hbar}\int \mathcal{E}_3(\vec{x}_3, t')e^{i\vec{k}_3\cdot\Delta\vec{x}_3(t')}e^{+(\Gamma_{10}-\Gamma_{20})\Delta t_3}dt' \ . \tag{11}$$

The assumption of weak excitation adopted here requires that $\theta_i \ll 1$ ($i = 1, 2, 3$). If the spectrum of

each of the exciting pulses is wide compared to the Doppler width of each corresponding transition the factor $\exp i(\vec{k}_i \cdot \Delta\vec{X}_i)$, which corresponds to a frequency shift $\vec{k}_i \cdot \vec{v}$, where $\vec{v}$ is the atomic velocity, may be ignored in the integral expression for θ_i. As a result, θ_i does not depend on the atomic velocity.

To determine when coherent emission of frequency ω_1 is generated by the medium at $t > t_3$ we calculate the macroscopic polarization $P(\vec{x}, t) = \langle \mathcal{N}\rho_{10}(\vec{x}, t) + \text{c.c.} \rangle$, where the brackets indicate an average over the atoms located at an arbitrary point $\vec{x}$ at the time t, and $\mathcal{N}$ is the atomic number density. The normalized Maxwell-Boltzmann velocity distribution is $f(\vec{v}) = \pi^{-3/2} v_0^{-3} \exp[-(\vec{v}/v_0)^2]$ where $v_0 = (2k_b T/M)^{-1/2}$, T is the absolute temperature, M the atomic mass, and k_b the Boltzmann constant. Since we assume that we may neglect velocity-changing collisions, an atom of velocity $\vec{v}$ which is at $\vec{x}$ at the time t was located at $\vec{x}_i = \vec{x} - \vec{v}(t - t_i)$ at the earlier time t_i. Carrying out the average over velocities we obtain

$$\langle \rho_{10}^{(1)}(\vec{x}, t) \rangle = \tfrac{1}{2} i \theta_1 e^{i(\vec{k}_1 \cdot \vec{x} - \omega_1 t)} e^{-\Gamma_{10}(t - t_1)} \times e^{-[k_1 v_0 (t - t_1)]^2} . \quad (12)$$

Clearly, this term gives a free decay with origin at $t = t_i$.

On the other hand, as we now show, the ensemble average $\rho_{10}^{(3)}(\vec{x}, t)$ contains a strong peak centered at a time t_e to be defined below; this will produce a SF-I echo of frequency ω_1 if $t_e > t_3$. Integrating $\rho_{10}^{(3)}(t)$ over the velocity distribution we have

$$\langle \rho_{10}^{(3)}(\vec{x}, t) \rangle = -\tfrac{1}{8} i \theta_1 \theta_2 \theta_3^* \exp\{-\Gamma_{10}[(t - t_3) + (t_2 - t_1)]\} \times e^{-\Gamma_{20}(t_3 - t_2)} e^{-|\vec{A}|^2 v_0^2/4} \times \exp\{i[(\vec{k}_1 + \vec{k}_2 - \vec{k}_3) \cdot \vec{x} - \omega_1 t]\} , \quad (13)$$

where

$$\vec{A} = (t - t_1)\vec{k}_1 + (t - t_2)\vec{k}_2 - (t - t_3)\vec{k}_3 . \quad (14)$$

For the collinear counterpropagating geometry of interest for which $\vec{k}_2 = \vec{k}_3$, it is found that $|\vec{A}| = 0$ at the time

$$t_e = t_1 + (t_3 - t_2) k_2/k_1 . \quad (15)$$

Therefore, at time t_e a macroscopic polarization of frequency ω_1 and wave vector $\vec{k}_1$ is formed in the medium. Let $\hat{z}$ lie along $\vec{k}_1$, and let $P = \mathcal{P} \exp[i(\vec{k}_1 \cdot \vec{x} - \omega_1 t)] + \text{c.c.}$ Using the slowly varying amplitude approximation for Maxwell's equation,

$$\left(\frac{\partial}{\partial z} + \frac{1}{c}\frac{\partial}{\partial t}\right)\mathcal{E} = 2\pi i k_1 \mathcal{P} , \quad (16)$$

and the expression for $\langle \rho_{10}^{(3)}(t) \rangle$ to find $\mathcal{P}$, one may easily show that a pulse of envelope maximum $\mathcal{E}_e \simeq 2\pi \mathcal{N} k_1 L |p_{01} \rho_{10}^{(3)}|_{\max}$, of frequency ω_1 and wave vector $\vec{k}_1$ is emitted at $t = t_e$. Hence

$$\mathcal{E}_e \simeq \tfrac{1}{4}\pi n k_1 L |p_{01} \theta_1 \theta_2 \theta_3^*| \times \exp\{-\Gamma_{10}[(t_e - t_3) + (t_2 - t_1)]\} e^{-\Gamma_{20}(t_3 - t_2)} , \quad (17)$$

where L is the length of the medium.

We note that the SF-I echo occurs only if $t_3 - t_2 \geq (t_3 - t_1) k_1/k_2$, so that $t_e \geq t_3$. A necessary condition for the formation of a SF-I echo is thus seen to be $k_2 > k_1$.

We should add that the *formation* of the SF-I echo and its dependence on the relaxation rates Γ_{10}, Γ_{20} does *not* depend on whether the various θ_i's are independent of $\vec{v}$ or whether $|\theta_i| \ll 1$. Indeed, we will show in Ref. 19 that for short unchirped pulses for which θ_i may be large, the value of $\rho_{10}^{(3)}(\vec{x}, t_e)$, neglecting relaxation and atomic motion during the pulses, is

$$\rho_{10}^{(3)}(\vec{x}, t) = -\tfrac{1}{2} i \sin|\theta_1| \sin|\tfrac{1}{2}\theta_2| \sin|\tfrac{1}{2}\theta_3| \times \exp\{i[(\vec{k}_1 + \vec{k}_2 - \vec{k}_3) \cdot \vec{x} - \omega_1 t]\} . \quad (18)$$

This expression shows that the weak-excitation formula (13) gives a good approximation (within several percent) to $\rho_{10}^{(3)}$ if $|\theta_1| \lesssim 0.2$, $|\theta_{2,3}| \lesssim 0.4$.

At this point we mention a characteristic of the SF-I echo which makes it especially suitable for measurements on highly excited states. Equation (18) predicts that the echo will be optimized when the pulse-area sequence is $\frac{1}{2}\pi - \pi - \pi$. With these angles and neglecting homogeneous decay, the peak electric field of the echo will, according to (17), be given by

$$\mathcal{E}_e \simeq \tfrac{1}{4}\pi n k_1 L |p_{01}| . \quad (19)$$

Hence the peak intensity $I_e = (c/2\pi)\mathcal{E}_e^2$ of the echo is *independent* of the oscillator strength of the 1-2 transition as long as the area under pulses 2 and 3 are maintained at π. Thus, neglecting homogeneous decay, the optimum SF-I echo will be approximately as intense as the optimum photon echo[20] on the $0 \rightarrow 1$ transition even if $|p_{12}| \ll |p_{01}|$. This result, which follows from the fact that the SF-I echo is *emitted* on the $0 \rightarrow 1$ transition, distinguishes it from other echo effects such as the excited-state photon echo,[21] which is emitted on the $1 \rightarrow 2$ transition. It means that SF-I echoes on states $|2\rangle$ with relatively weak dipole matrix elements p_{21} may be easily investigated. The only requirement is that $|\theta_{2,3}|$ must be maintained at a large value. As we have shown previously,[21] however, this is not very difficult with lasers of kilowatt peak power.

B. Echo decay and pressure broadening

The peak echo intensity I_e is given by

$$I_e = I_0 \exp\{-2\Gamma_{10}[(t_e - t_3) + (t_2 - t_1)]\} e^{-2\Gamma_{20}(t_3 - t_2)}, \tag{20}$$

where I_0 is a constant independent of the relaxation rates. We are interested in the dependence of I_e on the pressure p of a low-density ($p < 1$ Torr) foreign gas. The various phenomenological relaxation rates will be assumed to be linear in p as expected from a binary-encounter impact model. We therefore write

$$\Gamma_{ij} = \Gamma_{ij}^{(0)} = \eta_{ij} p , \tag{21}$$

where the collisional relaxation parameter η_{ij} has the units $\sec^{-1}\mathrm{Torr}^{-1}$.

The echo intensity therefore depends on p according to $I_e(p) \sim \exp(-\beta p)$, where

$$\beta = 2[\eta_{20} + \eta_{10}(k_2 - k_1)/k_1](t_3 - t_2) . \tag{22}$$

An interesting feature of this result is that the echo intensity does not depend on $t_2 - t_1$ (as long as $t_e > t_3$).

β may thus be determined by a measurement of echo intensity versus foreign-gas pressure at a fixed delay $t_3 - t_2$. Using a value of η_{10} measured by determining the pressure dependence of the 0-1 photon echo[20] at fixed delay time (see Table I) one can then obtain a value for η_{20}, the collisional relaxation parameter of the 0-2 superposition state.

We wish to relate Γ_{20} to the linewidth of the 0-2 transition, as would be measured by sweeping the monochromatic excitation frequency in a Doppler-free two-photon-absorption experiment. We consider the equation for ρ_{20} in the limit of weak ($\rho_{00} \gg \rho_{22}$) Doppler-free excitation by a monochromatic beam of frequency $\omega/2$ where $\omega \simeq \Omega_{20}$. ρ_{20} then satisfies

$$\left[\frac{\partial}{\partial t} + i(\Omega_{20} + \Delta_{20}) + \Gamma_{20}\right]\rho_{20} = -i\upsilon e^{-i\omega t} , \tag{23}$$

where $\upsilon = \text{const}$ is the effective field coupling levels 0 and 2, and Δ_{ij} is the collisional shift between levels i and j. The steady-state solution is

$$\rho_{20}(\omega) = \upsilon[(\omega - \Omega_{20} - \Delta_{20}) + i\Gamma_{20}]^{-1} e^{-i\omega t} \tag{24}$$

Hence the population

$$\rho_{22}(\omega) \simeq |\rho_{20}(\omega)|^2 = \upsilon^2[(\omega - \Omega_{20} - \Delta_{20})^2 + \Gamma_{20}^2]^{-1} ,$$

and the absorption line is Lorentzian with full width at half maximum (FWHM) $2\Gamma_{20}$. Thus the relaxation rate Γ_{20} of the superposition ρ_{20} as measured in a transient experiment is simply related to the Lorentzian linewidth measured by sweeping the excitation frequency in a steady-state experiment. By writing Γ_{20} as $\Gamma_{20}^{(0)} + \eta_{20} p$, we see that $2\eta_{20} p$ is the contribution to the linewidth of the collisions with the foreign gas. Similar considerations apply for Γ_{10} and η_{10}.

The average collisional shifts Δ_{10} and Δ_{20} will modify the echo intensity if they are large enough to shift the mean atomic transition frequencies outside the spectral profiles of the corresponding excitation pulses. In the experiments described here this is never the case, since Δ_{ij} is always much smaller than the spectral widths of the lasers. Therefore, we may ignore the pressure shifts.

It is customary to express $\eta_{ij} p$, the collisional contribution to Γ_{ij}, in terms of either a collisional rate constant K_{ij} ($\mathrm{cm}^3/\mathrm{sec}$) or an effective collisional cross section σ_{ij}. Let the foreign-gas number density be N. Then

$$\eta_{ij} p = NK_{ij} \equiv N\bar{V}\sigma_{ij} \tag{25}$$

Here $\bar{V}$, the average relative speed between the perturbating and the active atom, is given by $(8k_b T/\pi\mu)^{1/2}$, where μ is the reduced mass of the

TABLE I. Foreign-gas-induced collisional relaxation parameters for the sodium resonance lines measured using the photon-echo technique (see Ref. 21). Note that the FWHM of the collision-broadened line $\Delta\nu$ (Hz/Torr) $= \eta/\pi$. Alternately the broadening FWHM in cm^{-1} per relative density, $\Delta\tilde{\nu}$, is given by $\Delta\tilde{\nu} = 2.95 \times 10^{-11}\eta T$ cm^{-1}/r.d. where T is the absolute temperature. In the present work only the measurements for the $3\,^2S_{1/2}$-$3\,^2P_{1/2}$ transition were needed to determine the S-S and S-D relaxation rates. (All data was taken at a Na oven temperature of 400 ± 15 K.)

Superposition state	Foreign gas	η (sec Torr)$^{-1}$	Cross section (10^{-16} cm^2)
$3\,^2S_{1/2}$-$3\,^2P_{1/2}$	helium	49.1(1.5) $\times 10^6$	129(4)
	neon	28(3)	130(14)
	argon	57.3(2.9)	318(16)
$3\,^2S_{1/2}$-$3\,^2P_{3/2}$	helium	58.3(1.3)	153(4)
	argon	68.5(3)	380(17)

perturbing and active atom. Using the ideal gas law to relate p to N, we find $K_{ij} = \eta_{ij} k_b T = [1.04 \times 10^{-19}\ \mathrm{cm^3\,Torr/K}]\eta_{ij} T$.

III. EXPERIMENT

The apparatus used in our Na trilevel echo experiments is relatively simple and within reach of a modestly equipped laboratory. As shown in Fig. 3(a), the two homemade grating-tuned dye lasers of the Hänsch design are simultaneously pumped transversely by a single homemade nitrogen laser. The nitrogen laser, whose design is similar to one described by Nagata and Kimura,[22] produces 10-nsec long, 150-kW peak power 337-nm pulses at 5–20 Hz. Dye laser 1 is tuned such that $2\pi c/\omega_1 = 589$ nm, which is the wavelength corresponding to the Na $3\,^2S_{1/2}$-$3\,^2P_{1/2}$ ($|0\rangle$-$|1\rangle$) transition, and dye laser 2 ($410 < 2\pi c/\omega_2 < 615$ nm) is tuned to resonance between the $3\,^2P_{1/2}$ state and a higher $n\,^2S_{1/2}$ or $n\,^2D_{3/2}$ ($|2\rangle$) level (Fig. 1). Laser beam 1 at ω_1, whose spectral width is narrowed to ~1 GHz by an intracavity Fabry-Perot étalon, has a peak power of ~0.5 kW, while laser beam 2 at ω_2 has a peak power of ~3 kW and a spectral width of 10 GHz. Each laser beam is collimated by a 40-cm focal-length lens placed approximately a focal length beyond the respective dye cells. The beam of frequency ω_2 is split into two parts, one of which is optically delayed with respect to the other in a White cell.[23] The single pulse at ω_1 and the two subsequent pulses at ω_2, polarized by Glan-prism polarizers as indicated in Fig. 2(c), are incident on a heat-pipe-type stainless-steel cell containing metallic sodium in its central, oven-heated region. The central region of the cell is kept at a temperature of about 400 K, corresponding to a Na vapor pressure of $\simeq 10^{-5}$ Torr. Foreign gas may be introduced into the Na cell, and its pressure is measured by an MKS Baratron capacitance manometer. The time t_{21} ($t_{ij} = t_i - t_j$) between the peaks of the first two pulses was typically 5 nsec, while the delay $t_{32} \equiv \tau$ between pulses 2 and 3 was usually set to 41 nsec. As indicated in Figs. 2(b) and 3(a), the pulses at ω_1 and ω_2 counterpropagate; pulse 1 (ω_1) and 2 (ω_2) are (linearly) polarized vertically while pulse 3 ($\omega_3 = \omega_2$) is horizontally polarized. As a result (see Appendix B) the SF-I echo, a collimated pulse of wavelength $2\pi c/\omega_1$ which is emitted copropagating with pulse 1, is horizontally polarized [see Fig. 2(c)]. The echo is detected on an RCA C31034 photomultiplier tube (PMT). A horizontal polarizer placed in the path of the echo discriminates against pulse 1, while an interference filter centered at 589 nm discriminates against scattered

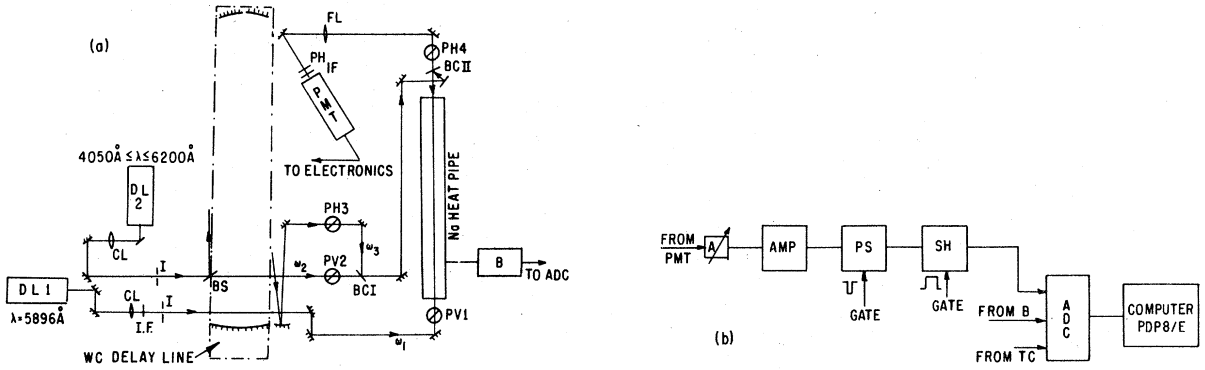

FIG. 3. (a) Schematic of experimental apparatus. Pumped by a single N_2 laser, dye lasers DL1 and DL2 are tuned, respectively, to the $|0\rangle$-$|1\rangle$ (ω_1) and $|1\rangle$-$|2\rangle$ ($\omega_2 = \omega_3$) transitions (see Fig. 1). Beam 1 (from DL1) passes through a bandpass filter (I.F.) and iris (I) to remove dye laser flourescence; then after being vertically polarized by PV1 (all polarizers are Glan prisms) it passes through the Na oven and is blocked by horizontal polarizer PH4. The output of DL2 is split at BS into beams 2 and 3. Beam 3 is delayed by an optical delay line (WC). After being polarized vertically (PV2) and horizontally (PH3), respectively, beams 2 and 3 are superimposed by BCI. Then using BCII beams 2 and 3 are sent through the sodium oven coincident with but counterpropagating with respect to beam 1. The echo, emitted along beam 1, passes through PH4 and is focused (FL) through a pinhole (PH) and bandpass filter (I.F.) which protect the RCA C31034 photomultiplier tube (PMT). An mks Baratron capacitance manometer (B) monitors foreign gas pressure in the Na cell. (b) Schematic of data-acquisition system. The echo signal from the PMT passes through a variable attenuator (A) and a ×100 amplifier (AMP) before being integrated by a gated pulse stretcher (PS). The output of the PS is read by a sample and hold (SH) and subsequently converted to digital format by an analog-to-digital converter (ADC). A PDP8/e minicomputer averages the digitized signal for a predetermined (approximately 100) number of echoes and stores the results. The thermocouple (TC)-monitored temperature and the pressure are also read (via the ADC) by the computer. The overall system is linear within 5% over approximately four orders of magnitude signal variation.

light from the pulses at ω_2. The elimination of the first pulse is crucial; an extinction of ~10^6, which is limited by depolarization of the room-temperature, fused-silica windows of the Na cell, is achieved. This extinction, coupled with the recovery characteristics of the PMT, allow us to observe an echo which is $\approx 10^8$ times less intense than the excitation pulse at ω_1. The fact that trilevel echoes can be detected using only crossed polarizers greatly reduces the difficulty of performing experiments which utilize them; the optical shutters necessary in most other pulsed echo experiments are generally difficult to work with on the time scale of our experiments. The PMT signal is fed into a gated pulse stretcher whose output is stored in a boxcar circuit and read into a DEC PDP 8/E computer [Fig. 3(b)]. The computer averages this signal over a number of laser shots, usually 75–125. This average signal and the computer-read value of the foreign-gas pressure are stored on a magnetic disc. An experimental run, lasting about 10–20 min, consists of the measurement of the echo signal at fixed delay as a function of the pressure, which is allowed to slowly leak up and then down so that the data may be continuously taken automatically. For a majority of the runs the delay τ between the two pulses at ω_2 was 41 nsec. In the few cases ($|2\rangle = 4D_{3/2}$ and $10S_{1/2}$ with Ar) in which τ was varied to some other value, it was always found that to within experimental error β scaled with τ as expected on the basis of simple exponential decay [see Eq. (22)].

For upper states ($|2\rangle$) with n less than ≈ 11 no lenses were used to focus the beams into the cell; the beam spot diameters were then about 2–3 mm. For higher n a 110-cm focal-length lens was used to focus the pulses at ω_2 to a diameter of ~1 mm in the cell.

Because of stray scattered light and electrical noise, the signal read by the computer, S, actually consists of a background signal S_2, as well as the echo signal. We determined S_2 by blocking the first excitation pulse at frequency ω_2. Since the PMT is protected by a bandpass filter at ω_1, we do not affect S_2 by blocking the pulse. Figure 4 shows the data points of several runs after S_2 has been subtracted. A logarithmic least-squares computer program is used to fit the data points of a given run to a curve of the form $S = S_1 \exp(\alpha_p p^2 - \beta p) + S_2$. S_1, α_p, and β are determined by the fit. Although we expect the echo to decay as a simple exponential with pressure (i.e., $\alpha_p = 0$), we find that our data is generally fit best with a small negative value of α_p. When we calculate the dimensionless quantity $(|\alpha_p|)^{1/2}/\beta$ we find that it has a fairly constant value of 0.1 to 0.15. At the present time we

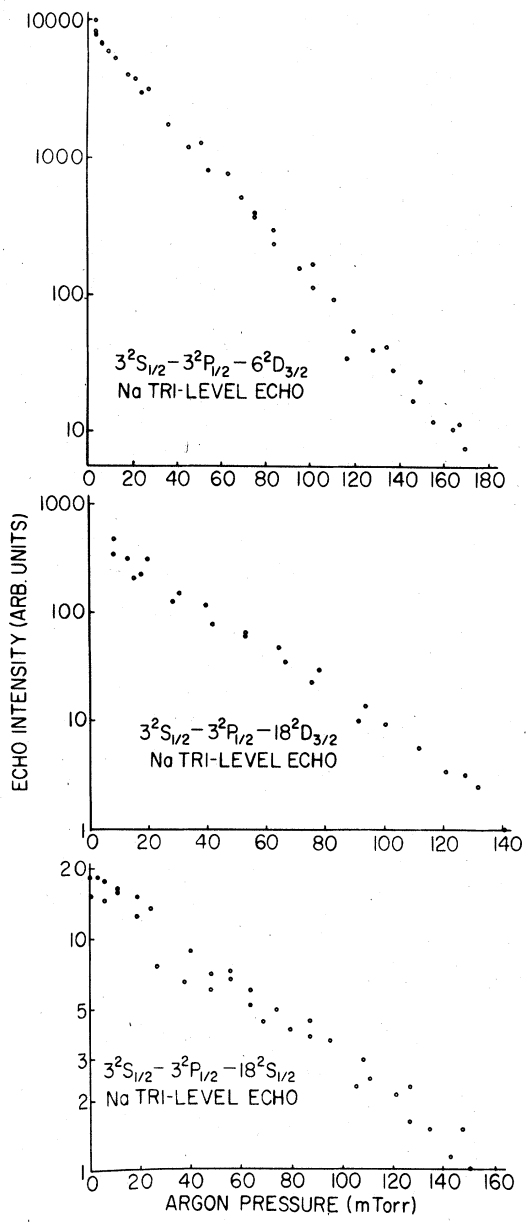

FIG. 4. Observed dependence of trilevel echo intensity on Ar pressure for three different $|2\rangle$ levels. The data points of each of the three runs shown above represent the average echo intensity produced over a fixed number of laser shots (typically 100). The data was taken continuously as the Ar pressure was first increased and then returned to its initial value.

do not know whether this behavior is due to systematic error or some unexpected physical aspect of the echo decay. The cross sections referred to in our discussion of results are derived from the fitted value of β. Because of the unknown origin of the α_p term, we must concede that a 10% systematic error may be hidden in our results. How-

ever, the relative errors from state to state, shown in the figures, are often smaller.

The ratio of S_1/S_2 was fairly constant at a value of 10^3–10^4 up to $n \simeq 11$. Above this point it slowly decreased, reaching a value of ~2 for $n = 34$. We interpret the decrease in echo intensity as we proceed to the higher states as evidence that our excitation pulses at ω_2 resonant with the $|2\rangle$-$|1\rangle$ transition were no longer sufficiently intense (due to the decreasing oscillator strength of the $1 \rightarrow 2$ transition and the fact that our laser dyes and dielectric reflective coatings did not perform well at the relevant wavelengths) to transfer a sizeable population from state 1 to 2 and back (i.e., $|\theta_2| \simeq |\theta_3| < \pi$). The use of a lens to focus the beams at ω_2 to a smaller spot (and hence larger peak intensity) increased the echo signal somewhat at these higher $|2\rangle$ states, but the gain was partially offset by the smaller volume of Na atoms excited by the laser beams.

TABLE II. Measured foreign-gas-induced collisional relaxation parameters. Note that η in this table can be expressed in the nomenclature of NMR as $1/(T_2)_{fg}$ where $(T_2)_{fg}$ is the per Torr transverse relaxation time due to the foreign gas. The numbers in parenthesis represent the statistical error of our data. See text for a discussion of possible systematic error. (All data were taken at a Na oven temperature of 400 ± 15 K.)

Superposition state	η (sec Torr)$^{-1}$ argon	neon	helium
$3\,^2S_{1/2}$-$5\,^2S_{1/2}$	237×10^6	···	300×10^6
$3\,^2S_{1/2}$-$6S$	315	93×10^6	373
$3\,^2S_{1/2}$-$7S$	444(29)	56(3)	285(14)
$3\,^2S_{1/2}$-$8S$	479	50	189
$3\,^2S_{1/2}$-$9S$	395	40	144
$3\,^2S_{1/2}$-$10S$	381(14)	45(6)	109(7)
$3\,^2S_{1/2}$-$11S$	307	43	84
$3\,^2S_{1/2}$-$12S$	254	41	74
$3\,^2S_{1/2}$-$13S$	249	56	73
$3\,^2S_{1/2}$-$14S$	245	46	57
$3\,^2S_{1/2}$-$15S$	201(10)	47(6)	56(4)
$3\,^2S_{1/2}$-$16S$	209	47	63
$3\,^2S_{1/2}$-$17S$	167	35	71
$3\,^2S_{1/2}$-$18S$	188(15)	46(6)	54(4)
$3\,^2S_{1/2}$-$19S$	202	48	···
$3\,^2S_{1/2}$-$20S$	133	···	···
$3\,^2S_{1/2}$-$4\,^2D_{3/2}$	192	82	149
$3\,^2S_{1/2}$-$5D$	293	92	172
$3\,^2S_{1/2}$-$6D$	489	103	216
$3\,^2S_{1/2}$-$7D$	665(28)	98(5)	263(14)
$3\,^2S_{1/2}$-$8D$	829	106	279
$3\,^2S_{1/2}$-$9D$	872	104	324
$3\,^2S_{1/2}$-$10D$	848(59)	97(7)	360(8)
$3\,^2S_{1/2}$-$11D$	759	90	351
$3\,^2S_{1/2}$-$12D$	724	81	351
$3\,^2S_{1/2}$-$13D$	690	81	299
$3\,^2S_{1/2}$-$14D$	604	72	273
$3\,^2S_{1/2}$-$15D$	584(25)	73(4)	276(11)
$3\,^2S_{1/2}$-$16D$	487	53	232
$3\,^2S_{1/2}$-$17D$	445	59	215
$3\,^2S_{1/2}$-$18D$	420(48)	59(12)	209(25)
$3\,^2S_{1/2}$-$19D$	389	48	···
$3\,^2S_{1/2}$-$20D$	320		
$3\,^2S_{1/2}$-$21D$	278		
$3\,^2S_{1/2}$-$22D$	249		
$3\,^2S_{1/2}$-$23D$	270		
$3\,^2S_{1/2}$-$24D$	251		
$3\,^2S_{1/2}$-$25D$	279		
$3\,^2S_{1/2}$-$26D$	128		
$3\,^2S_{1/2}$-$27D$	177(33)		
$3\,^2S_{1/2}$-$34D$	178		

The values of β for several runs with the same foreign gas were averaged for each state, and the means used to calculate values of η_{20} and collisional cross sections according to (22) and (25). Our values of the η's are tabulated in Table II.

It will be noted that experimental cross sections σ_{20} are tabulated for the collisional relaxation of the $3\,^2S_{1/2}$-$5\,^2S_{1/2}$ superposition. According to the theory outlined above, however, the SF-I echo *cannot occur* on the $3\,^2S_{1/2}$-$3\,^2P_{1/2}$-$5\,^2S_{1/2}$ levels, since $k_2 < k_1$. The undelayed ($t_e \simeq t_3$) echoes which were observed on this transition, and which were used to determine the σ_{20}'s arise from a *different* type of trilevel echo, the type-II sum-frequency trilevel (SF-II) echo, whose excitation scheme is identical to that described above. It is explained in Appendix C.

IV. DISCUSSION OF RESULTS

The tri-level echo decay cross sections derived from the η's of Table II for Na-He, Na-Ne, and Na-Ar collisions are shown in Fig. 5(a), 5(b), and 5(c), respectively. In almost all cases our data is the first ever obtained for the various superposition states. In Table III we compare our trilevel echo decay cross sections with the few previously reported broadening and transient decay cross sections. Note (assuming the temperature dependence of the cross sections is weak) that the agreement between the values is quite good. This tends to confirm our phenomenological analysis of the relationship between echo decay and line broadening.

We see from Fig. 6 that our cross sections vary with n in a fashion similar to that observed in previous measurements of the foreign-gas-induced broadening of the principal series transitions in the alkalis.[1-3,5] Although one might be tempted to say that the collisional cross sections should vary as the geometrical cross section of the excited alkali atom ($\pi n^{*2} a_0^2$ where $a_0 = 0.53$ Å is the Bohr radius and n^* the effective principal quantum number), a simple argument provides an explanation of the gross features of the observed n dependence of the collisional cross section.

Consider a collision between a noble-gas atom

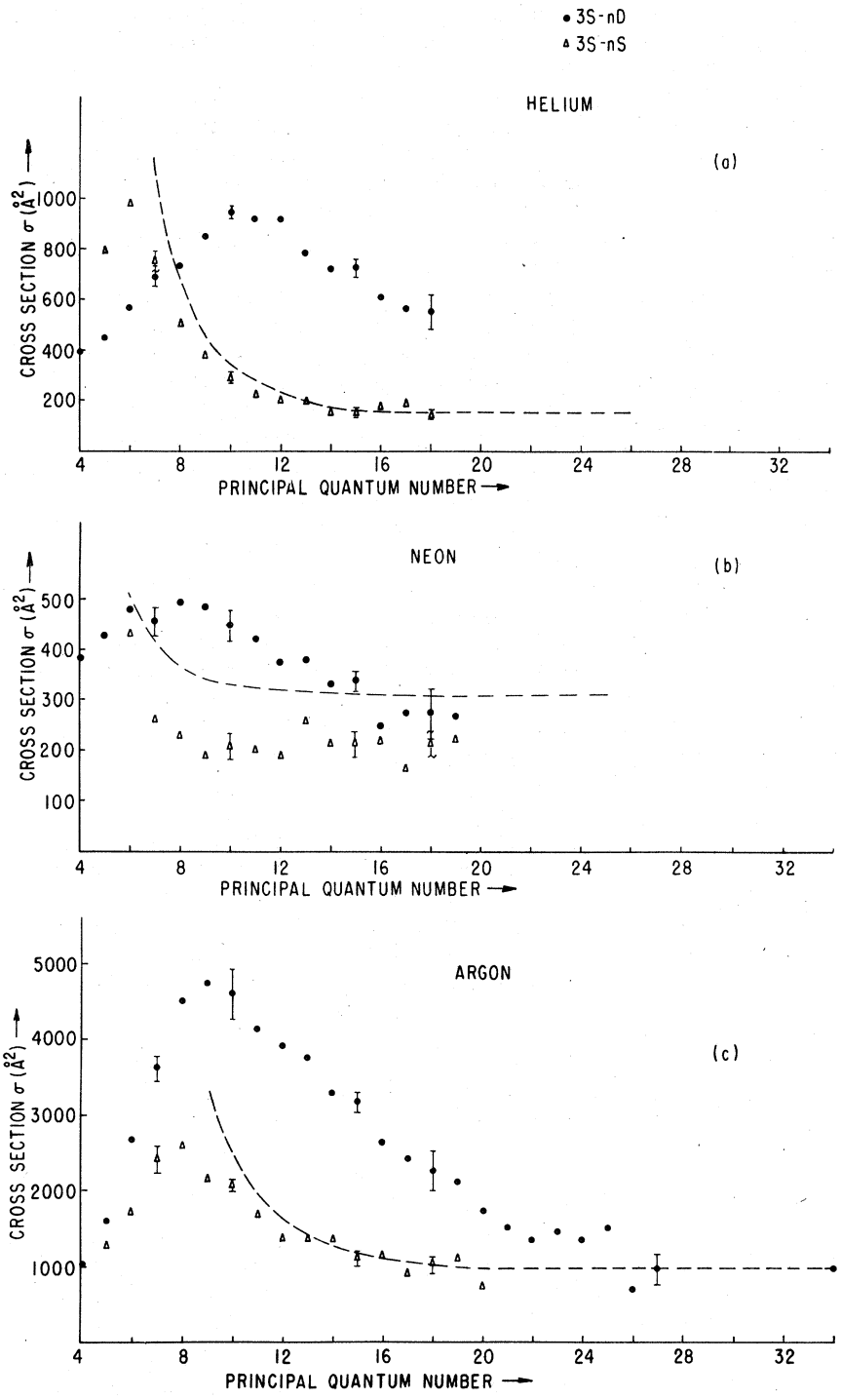

FIG. 5. Collisional cross sections derived from our trilevel echo relaxation data. Points shown represent our measured values of σ, while the dashed lines correspond to the values predicted by Omont (Ref. 9) for the $3\,^2S_{1/2}-n\,^2S_{1/2}$ superposition states. The errors shown are typical and represent the statistical error of our data. See text for a discussion of possible systematic error.

F of speed $\bar{V}$ and a stationary alkali atom in an excited state of effective quantum number n^*. The alkali-metal atom consists of a valence electron e^- circulating rapidly about a stationary, positive Na^+ core. Within the limitations imposed by the uncertainty principle, the electron is a distance $r = a_0(n^*)^2$ from the core and is moving at a speed $v_e = \alpha c/n^*$.[24] Here α is the fine-structure constant and c is the speed of light. For the lower states (n^* small) one must treat the alkali atom as a unit in calculating the scattering. Since the Van der Waal interaction increases with n^*, the

TABLE III. Comparison of the 3S-4D and 3S-5S foreign-gas-induced broadening cross sections, which have been obtained by different experimental techniques.

Superposition state	Foreign gas	Cross section ($\times 10^{-16}$ cm^2)			
		Biraben *et al.*[a]	Liao *et al.*[b]	Two-photon echo[c]	Trilevel echo measurement[d]
3S-4D	helium	407(48)	386(32)	...	391(16)
	neon	399(28)	304(28)	...	382(13)
	argon	1045(109)	1042(67)	970(149)	1045(174)
3S-5S	helium	722(32)	...	...	788(45)
	neon	493(37)	...	...	...
	argon	1182(88)	...	...	1286(93)

[a] Obtained from measurements (at $T=563$ K) of Doppler-free two-photon absorption linewidth broadening (Ref. 12).
[b] Obtained from measurements of the Doppler-free two-photon coherent transient of Ref. 13 (at $T=673$ K).
[c] Measured at $T=400$ K (Ref. 14).
[d] Our trilevel echo measurements at $T=400$ K.

scattering cross section increases as n^* is increased. For higher n, however, a different effect comes into play. The Na^+ core and (quasifree) valence electron are so far apart that they scatter the incoming noble-gas atom independently. Defining the cross section for the two types of collisions by $\sigma_e(v_e)$ and σ_{Na^+}, respectively, and restricting ourselves to the limit $\overline{V} \ll v_e$, we can estimate the total collision rate constant K_{tot} and collision cross section $\sigma_{tot} = K_{tot}/\overline{V}$ as

$$K_{tot} \simeq \overline{V}\sigma_{Na^+} + v_e\sigma_e(v_e) \tag{26}$$

and

$$\sigma_{tot} \simeq \sigma_{Na^+} + v_e\sigma_e(v_e)/\overline{V}\,. \tag{27}$$

With increasing n the second term decreases as $1/n$ if $\sigma_e(v_e)$ is nearly constant. This naive picture explains, at least qualitatively, the observed dependence of the cross section on n. Indeed, it predicts that $\sigma_{tot} \to \sigma_{Na^+}$ asymptotically as n increases.

In an attempt to explain the data of Füchtbauer and Schulz,[1] Alekseev and Sobelman[6,8] have calculated σ_{tot} in the asymptotic limit for $Na(n^2P)$-Ar collisions. Their more rigorous approach is along the lines of (27), with two exceptions: (a) they include the exchange interaction and (b) for the e^--Ar collision σ_e increases sharply with decreasing velocity v_e; hence they find that it is more appropriate to average the expression for K_{tot} over the velocity distribution of the quasifree electron. In spite of these complications they find that the con-

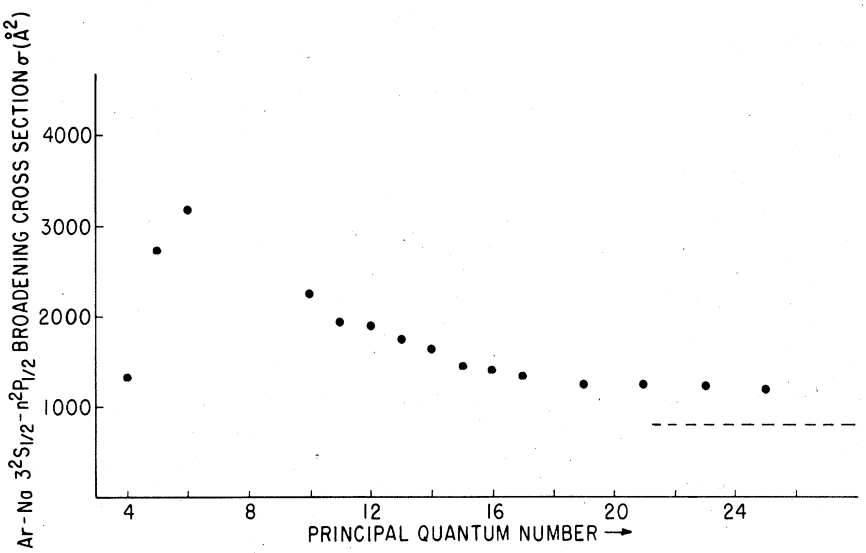

FIG. 6. Collisional broadening cross sections observed by Füchtbauer and Shulz (Ref. 1) for the principal series of Na perturbed by Ar. Dashed curve represents the asymptotic limit predicted in Refs. 8 and 9.

tribution of the e^--Ar scattering is significantly smaller than that of Na^+-Ar. This justifies our rough estimate that σ_{Na^+} should be the proper asymptotic limit even when F = Ar. We note that Gounand, Fournier, and Berlande[25] have made a similar calculation, except that they determine the mean speed v_e of an electron in a state n from

$$v_e = \int_0^\infty v f_n(v)\, dv ,$$

where $f_n(v)$ is the velocity distribution of the electron in state n, instead of using the rms speed $v_e \simeq \alpha c/n^*$, as we have. As one expects for highly excited states, the two speeds are only ~10% apart, hence their results are nearly identical with ours.

Recently an attempt has been made for the first time to make quantitative estimates of the noble-gas-induced collisional cross sections for states with n below the asymptotic limit. Omont[9] concludes, as did previous workers, that in the asymptotic limit the interaction between the noble-gas atom and the alkali-metal atom is dominated by the valence-electron-state-independent polarization of the noble-gas atom induced by the positively charged core of the alkali-metal atom. To calculate the collisional broadening for transitions involving upper states of lower n Omont has made an approximate calculation of the effect of the electron–noble-gas potential as well as the polarization potential. He treats the potentials as additive and assumes that each dominates for certain values of the collisional impact parameter. For very low n this method fails because the collision becomes truly three body; however, it appears to give approximate agreement with experiment in certain circumstances. The dashed lines in Fig. 5 indicate the effective trilevel echo decay cross sections expected based on Eqs. (4.14) –(4.17) and appropriate constants given in Ref. 9. In the cases of the superpositions involving the energetically isolated s states as the upper level with either He or Ar as the perturbing gas the theory predicts cross sections quite close to those we observe. Since the calculation treats only elastic collisions it is not surprising that the superpositions involving the nearly degenerate d states have collisional cross sections higher than predicted (see below). The case of Ne is anomalous: The theory gives cross sections which are significantly above the experimental values for all values of n—even in the asymptotic region. Except for the fact that the ratio $(|\alpha_p|)^{1/2}/\beta$ (see Sec. III) was slightly larger than for He or Ar our experimental values for Ne should be of roughly the same quality as for the other foreign gases. In fact as shown in Table III our measurements of the Na-Ne collision decay cross section for the 3S-4D superposition are in good agreement with the measurements of Biraben *et al.*[12] We thus conclude that either there is a hidden error in our Ne-Na collisional cross sections for higher n or the existing theories are not sufficiently general to describe the interaction involved in Na-Ne collisions.

Although the collision cross sections for the S-S superposition states are expected[9,16,17] to be almost entirely due to elastic collisions, measurements by Gallagher, Edelstein, and Hill[16] show that a sizable part of the collision cross section for the S-D superpositions must be due to collisionally induced transfer of population out of the upper state. The collision transfer cross sections σ_{CT} measured by Gallagher imply that during the interval t_{32} the upper d state is depleted in population by the factor $\exp(-N\bar{V}\sigma_{CT}t_{32})$. Thus, neglecting decay mechanisms other than population transfer, ρ_{20} decays by a factor $\exp(-N\bar{V}\sigma_{CT}t_{32}/2)$ and $\sigma_{20} = \sigma_{CT}/2$. In Fig. 7 we plot our trilevel echo S-D collision cross sections σ_{20} (solid circles) along with one half the inelastic-collision cross sections measured by Gallagher (open triangles). In the presence of elastic collisions we expect σ_{20} to be larger than $\sigma_{CT}/2$, and indeed in most cases it is significantly larger. Since in the case of He $\sigma_{CT}/2$ and σ_{20} are nearly equal for the higher d states, we conclude that in those cases inelastic collision are dominant.

In the limit of large n^* the cross section for elastic collisions should become independent of the electron's orbital angular momentum l. The same statement holds true for the collision-transfer cross section.[9] In the region we work n^* is large enough for the first statement to be valid, but not the second. In fact for the states we measure σ_{CT} is generally negligible for n^*S but appreciable for n^*D states. In consideration of these facts the difference $\Delta\sigma = \sigma_{20}(S\text{-}n^*D) - \sigma_{20}(S\text{-}n^*S)$ should be a good measure of the collision-transfer cross section, i.e., $\Delta\sigma$ should be nearly equal to $\sigma_{CT}/2$. We have computed the difference cross sections $\Delta\sigma$ from our data and plotted them (crosses) in Fig. 7. We find (except in the case of He) that especially for large n^* the agreement between $\Delta\sigma$ and $\sigma_{CT}/2$ is striking. On the other hand for He $\sigma_{20}(S\text{-}n^*D)$ itself agrees so well with $\sigma_{CT}/2$ that the subtraction of $\sigma_{20}(S\text{-}n^*S)$ to obtain $\Delta\sigma$ actually reduces the agreement. This implies that either $\sigma_{20}(S\text{-}n^*S)$ contains a significant contribution from inelastic collisions or interference between the elastic and inelastic contribution to the cross section is occurring. For very low n^* $\Delta\sigma$ becomes negative implying that the assumption of l independence of the elastic cross section must break down. The possibility that $\Delta\sigma$ can be used to ob-

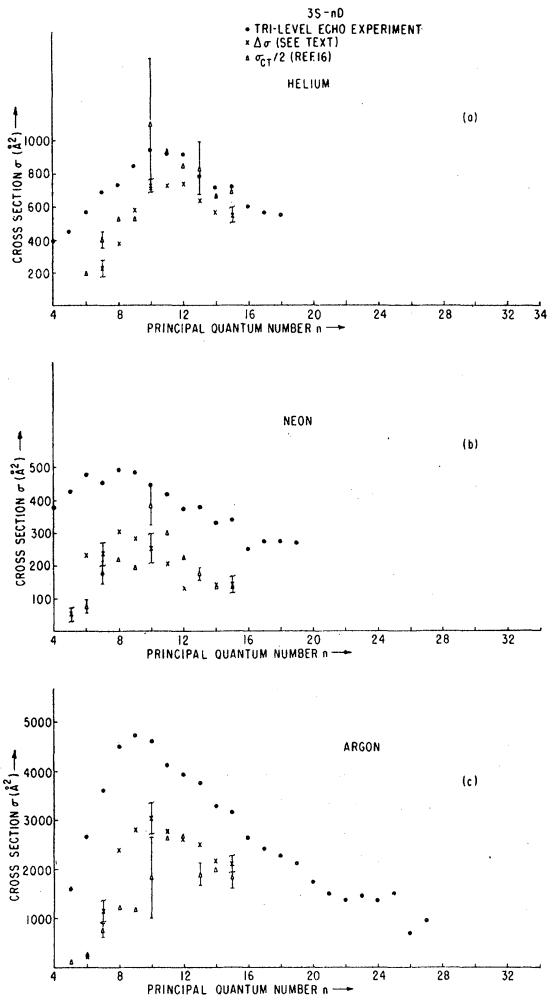

FIG. 7. Comparison of $\frac{1}{2}$ the collisional transfer cross sections (open triangles) given in Ref. 16 and the difference between the total $3S$–n^*D and $3S$–n^*S collision cross sections $\Delta\sigma$ measured by the trilevel echo technique (crosses). The collisional transfer cross sections of Ref. 16 are multiplied by $\frac{1}{2}$ to give the effective trilevel echo decay cross sections due to population transfer out of the D state (see text). To obtain these values of $\Delta\sigma$ we used pointwise linear interpolation to obtain the total $3S$–n^*S collision cross sections from those measured for the $3S$–nS superpositions. It is found that the use of n in place of n^* does not significantly alter the values of $\Delta\sigma$ shown here. Also included in this figure are our measured values for the total $3S$–nD collision cross sections (solid circles). The error bars shown are typical.

tain the inelastic collision cross section certainly warrants further investigation.

V. CONCLUSION

We have measured the foreign-gas-induced relaxation characteristics of $3S$-nS and $3S$-nD superposition states in Na for a large range of n. For the cases where n is in the Rydberg regime our measurements are the first ever made. The measurements are interesting in that they clearly show the effect of the near degeneracy of the d states of higher l but the same n. This contrasts with the energetically isolated s states. We have compared the recently presented theoretical work of Omont[9] with our measurements of the relaxation of $3S$-nS superposition states. The agreement is good except when Ne is used as the foreign gas.

By making these measurements we have demonstrated the power of the trilevel echo effect when applied to relaxation measurements. We plan to extend our studies to higher n, to other foreign gases, and to other alkali metals. In the cases of the heavier alkali metals where the necessary $|1\rangle$-$|2\rangle$ excitation frequencies lie in regions where more efficient laser dyes are available we expect to be able to reach states of significantly higher n.

ACKNOWLEDGMENTS

This work is supported by the Joint Services Electronics Program (U.S. Army, U.S. Navy, U.S. Air Force) under Contract No. DAAG29-77-C-0019 and the Office of Naval Research under Contract No. N00014-78-C-0517.

APPENDIX A

In this Appendix we consider the formation of the SF-I echo when states $|0\rangle$, $|1\rangle$, and $|2\rangle$ each represents a manifold of nearly degenerate levels $|a_i\rangle$, $|b_i\rangle$, and $|c_i\rangle$. We limit our discussion to weak excitation. The laser electric fields are now considered vector quantities. The initial nonzero density matrix elements are $\rho_{a_ia_j}=g_0^{-1}$, where g_0 is the number of levels (assumed to all be equally populated) in the ground-state manifold. During the first pulse Eq. (3) is now replaced by

$$\left(\frac{\partial}{\partial t}+i\Omega_{b_ia_j}+\Gamma_{10}\right)\rho_{b_ia_j}=\frac{i}{\hbar}g_0^{-1}\vec{\mathrm{p}}_{b_ia_j}\cdot\vec{\mathbf{E}}(\vec{\mathbf{X}},t)\,. \tag{A1}$$

Here $\Omega_{b_ia_j}\simeq\Omega_{10}=\omega_1$ is the energy separation between levels b_i and a_j, and the phenomenological relaxation rate Γ_{10} is assumed to be identical for all elements $\rho_{b_ia_j}$. After the first pulse $\rho_{b_ia_j}$ is given by

$$\rho^{(1)}_{b_ia_j}=\tfrac{1}{2}ig_0^{-1}\theta_1(b_i,a_j)e^{i(\vec{\mathrm{k}}_1\cdot\vec{\mathrm{x}}_1-\Omega_{b_ia_j}t)}e^{-\Gamma_{10}(t-t_1)} \tag{A2}$$

where

$$\theta_1(b_i,a_j)=2\frac{\vec{\mathrm{p}}_{b_ia_j}}{\hbar}\cdot\int\vec{\mathcal{E}}_1(\vec{\mathrm{x}}_1,t')\times\exp\{i[\vec{\mathrm{k}}_1\cdot\Delta\vec{\mathrm{X}}_1(t')-(\omega_1-\Omega_{b_ia_j})t']\}\times e^{+\Gamma_{10}\Delta t_1}\,dt'\,. \tag{A3}$$

Similarly, after the second pulse we find in analogy with (7) that

$$\rho_{c_i a_j} = -\tfrac{1}{4} g_0^{-1} \sum_l \theta_2(c_i, b_l)\theta_1(b_l, a_j) \times \exp\{i[\vec{k}_1\cdot\vec{x}_1 + \vec{k}_2\cdot\vec{x}_2 - \Omega_{c_i a_j} t]\} \times e^{-\Gamma_{20}(t-t_2)} e^{-\Gamma_{10}(t_2-t_1)}, \quad \text{(A4)}$$

where

$$\theta_2(c_i, b_l) = \frac{2\vec{p}_{c_i b_l}}{\hbar}\cdot\int \vec{\mathcal{E}}_2(\vec{x}_2, t') \times \exp\{i[\vec{k}_2\cdot\Delta\vec{X}_2(t') - (\omega_2 - \Omega_{c_i b_l})t']\} \times e^{-(\Gamma_{10}-\Gamma_{20})\Delta t_2'}\, dt'.$$

Finally, the term $\rho^{(3)}_{b_i a_j}$ of $\rho_{b_i a_j}$ which produces the trilevel echo is given by

$$\rho^{(3)}_{b_i a_j} = \frac{-i}{8} g_0^{-1} \sum_{l,m} \theta_3^*(c_m, b_i)\theta_2(c_m, b_l)\theta_1(b_l, a_j) \exp\{i[\vec{k}_1\cdot\vec{x}_1 + \vec{k}_2\cdot\vec{x}_2 - \vec{k}_3\cdot\vec{x}_3 - \Omega_{b_i a_j} t]\} \times e^{-\Gamma_{10}(t-t_3)} e^{-\Gamma_{20}(t_3-t_2)} e^{-\Gamma_{10}(t_2-t_1)}, \quad \text{(A5)}$$

where

$$\theta_3(c_m, b_i) = \frac{2\vec{p}_{c_m b_i}}{\hbar}\cdot\int \vec{\mathcal{E}}_3(\vec{x}_3, t') \exp\{i[\vec{k}_3\cdot\Delta\vec{X}_3(t') - (\omega_2 - \Omega_{c_m b_i})t']\}\, e^{-(\Gamma_{10}-\Gamma_{20})\Delta t_3'} dt' . \quad \text{(A6)}$$

As before the polarization at the echo time t_e is then

$$\vec{P}(\vec{x}, t_e) = \mathfrak{N} \sum_i \vec{p}_{b_i a_j} \langle \rho^{(3)}_{b_i a_j}(\vec{x}, t_e)\rangle + \text{c.c.} . \quad \text{(A7)}$$

Equation (A7) can be used as the starting point for a calculation of the polarization of the echo (Appendix B) and of "quantum-beat" effects in the echo due to t_e-dependent interference between the terms summed over.

APPENDIX B

Using the results [(A5) and (A7)] of Appendix A, which are valid in the weak-excitation limit, we calculate the polarization of the SF-I echo for the choice of excitation pulse polarizations depicted in Fig. 2(c). We will show that the echo is polarized perpendicular to the first pulse.

We choose to quantize along the linear polarization of pulse 1, so that $\vec{E}_1 = E_1\hat{z}$, $\vec{E}_2 = E_2\hat{z}$, $\vec{E}_3 = E_3\hat{x}$; the direction of propagation of pulse 1 (and the echo) is $\hat{y}$. The states are now designated by $|lJ_l m_l\rangle$, where $l = 0, 1, 2$ denotes the manifold, while J_l, m_l are the quantum numbers of the total and axial angular momentum, respectively. From Eq. (A7) we have

$$\vec{P}(\vec{x}, t_e) = n \sum_{\substack{m_0, m_1 \\ \alpha}} \langle 0 J_0 m_0 | p_\alpha \hat{\epsilon}_\alpha | 1 J_1 m_1\rangle \times \langle 1 J_1 m_1 | \rho^{(3)}(\vec{x}, t_e) | 0 J_0 m_0\rangle + \text{c.c.}, \quad \text{(B1)}$$

where

$$\langle 1 J_1 m_1 | \rho^{(3)} | 0 J_0 m_0\rangle \sim \sum_{\substack{m_2, m_1' \\ \beta}} \langle 1 J_1 m_1 | p_\alpha a_\beta | 2 J_2 m_2\rangle \times \langle 2 J_2 m_2 | p_0 | 1 J_1 m_1'\rangle \times \langle 1 J_1 m_1' | p_0 | 0 J_0 m_0\rangle \quad \text{(B2)}$$

Here $\hat{\epsilon}_\alpha (\alpha = 0, \pm 1)$ is a unit vector of circular polarization; it follows from the choice $\vec{E}_3 = E_3\hat{x}$ that $a_{\pm 1} = \mp 1/\sqrt{2}$; $a_0 = 0$. Combining Eqs. (B1) and (B2) and applying the Wigner-Eckart theorem to this expression, we find

$$\vec{P}(\vec{x}, t_e) \sim |(0 J_0 \| p \| 1 J_0)(1 J_0 \| p \| 2 J_2)|^2 \times \sum_{\substack{m_0 m_1 \\ m_2 m_1'}} \sum_{\alpha\beta} \hat{\epsilon}_\alpha a_\beta \langle J_0 m_0 | 1 J_1 \alpha m\rangle \langle J_1 m_1 | 1 J_2 \beta m_2\rangle \times \langle J_2 m_2 | 1 J_1 0 m_1'\rangle \langle J_1 m_1' | 1 J_0 0 m_0\rangle \quad \text{(B3)}$$

where $\langle\,|\,\rangle$ is a Clesbsch-Gordan coefficient and $(\|\,\|)$ a reduced dipole matrix element.[26] The selection rules imply that only those terms with $m_2 = m_1' = m_0$ are nonzero. Since $a_0 = 0$ we must have $m_1 = m_0 \pm 1$, hence only terms with $\alpha = \pm 1$ may contribute. Therefore $\vec{P} = P_x\hat{x} + P_y\hat{y}$. Since the echo propagates along $\hat{y}$ it must be polarized along $\hat{x}$.

A very simple argument, based on conservation of the z component of angular momentum of the light, leads to the same result. The photons of the first and second pulses carry 0 units of angular momentum along $\hat{z}$, while those of the third pulse carry ± 1 units. Thus the echo will radiate photons with ± 1 units of angular momentum in order for the atoms to return to their initial state, as they must in any process in which the coherence between atoms is crucial. This shows that none of the echo photons can carry 0 units of angular momentum along $\hat{z}$, i.e., the echo must be

polarized normal to $\hat{z}$. Since the echo propagates along $\hat{y}$, it must be polarized along $\hat{x}$.

APPENDIX C

Consider the pulse sequence shown in Fig. 8(a), where $k_2 < k_1$, and $\vec{k}_2$ and $\vec{k}_1$ are antiparallel. This sequence is identical to that which produces the SF-I echo, except that we now require that the first pulse at ω_2 overlap temporally with the pulse at ω_1. The calculation of Sec. II indicates that no SF-I echo is formed at $t \geq t_3$ in this case. We now show that if the ratio of the pulsewidth Δt to the dealy t_{32} is greater than a critical value which depends on k_2/k_1, a different trilevel echo, of frequency ω_1 and wave vector $\vec{k}_1$, is produced at $t_e \approx t_3$. We refer to this new echo, which we reported but were unable to explain previously as a sum-frequency trilevel echo type II (SF-II echo).

In order to explain the formation of a SF-II echo, we replace the three-pulse sequence of Fig. 8(a) by the four-pulse sequence of Fig. 8(b) and calculate the value of $\rho_{10}(\vec{x}, t)$ for $t \geq t_3$. We again restrict the calculation to the weak-excitation limit. The four pulses are temporally distinct, but at the end of the calculation, we take the limit t_1, $t_1' \to t_2$, so that the sequence of Fig. 8(b) will approach that of Fig. 8(a). Our reason for using this approach will become clear below.

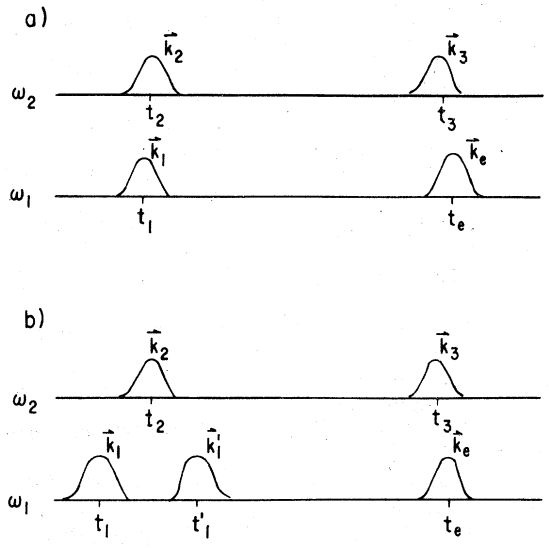

FIG. 8. (a) Temporal sequence of actual excitation pulses and echo for the SF-II echo. The excitation pulses at t_1 and t_2 of frequencies ω_1 and ω_2, respectively, are required to have temporal overlap. An echo occurs for $t_e \cong t_3$ if $k_1 \cong k_2$. (b) Temporal sequence of excitation pulses used in the analysis of the SF-II echo. The pulse at t_1 is involved only in that it places population in level $|1\rangle$. The scheme of (a) is reached by letting t_1 and t_1' approach t_2.

Our procedure will be as follows: we calculate the population ρ_{11} excited by pulse 1. Then we find the value of ρ_{21} produced by pulse 2, and calculate the value of ρ_{20} produced by pulse 1′. Finally, we find the change in ρ_{21} brought about by pulse 2 and investigate its rephasing properties. Since we eventually let the first three pulses approach each other, we neglect relaxation during the interval between pulses 1, 2, and 1′. After pulse 1, ρ_{10} is given by Eq. (4), hence $\rho_{11} \simeq |\rho_{10}|^2 = \frac{1}{4}|\theta_1|^2$. Pulse 2 modifies ρ_{21} according to

$$\left(\frac{\partial}{\partial t} + i\Omega_{21}\right)\rho_{21} = \frac{-i}{\hbar} p_{21} E_2 \rho_{11} \,. \tag{C1}$$

Hence after pulse 2

$$\rho_{21} = -\tfrac{1}{8} i\theta_2 |\theta_1|^2 e^{i(\vec{k}_2 \cdot \vec{x}_2 - \Omega_{21} t)} \,. \tag{C2}$$

Pulse 1′ modifies ρ_{20} according to

$$\left(\frac{\partial}{\partial t} + i\Omega_{20} + \Gamma_{20}\right)\rho_{20} = -\frac{i}{\hbar} p_{10} E_1' \rho_{21} \tag{C3}$$

producing a term ρ_{20}' in ρ_{20} which is given by

$$\rho_{20}'(t > t') = -\tfrac{1}{16}\theta_1'\theta_2|\theta_1|^2 \exp[i(\vec{k}_2 \cdot \vec{x}_2 + \vec{k}_1' \cdot \vec{x}_1' - \Omega_{20} t)] \times e^{-\Gamma_{20}(t - t_1')} \,. \tag{C4}$$

We may now find the effect of pulse 3 on ρ_{10}, which, during and after pulse 3 satisfies

$$\left(\frac{\partial}{\partial t} + i\Omega_{10} + \Gamma_{10}\right)\rho_{10} = \frac{i}{\hbar} p_{12} E_3^* \rho_{20} \,. \tag{C5}$$

We are interested only in the term ρ_{10}' in ρ_{10} which arises from ρ_{20}'. It is given for $t > t_3$ by

$$\rho_{10}' = -\tfrac{1}{32} i\theta_1'\theta_2|\theta_1|^2 \times \exp[i(\vec{k}_2 \cdot \vec{x}_2 + \vec{k}_1' \cdot \vec{x}_1' - \vec{k}_3 \cdot \vec{x}_3 - \Omega_{10} t)] \times \exp\{[\Gamma_{10}(t - t_3) + \Gamma_{20}(t_3 - t_1')]\} \,. \tag{C6}$$

Substituting $\vec{k}_3 = \vec{k}_2 = -k_2\hat{z}$, $\vec{k}_1' = k_1'\hat{z}$, $\vec{x}_i = \vec{x} - \vec{v}(t - t_i)$ in the above expression, we find that complete rephasing occurs when $t = t_e \equiv (k_2/k_1)(t_3 - t_2) + t_1'$. The rephasing will only be real if the value of t_e determined from this definition is at least as large as t_3. This requires that

$$t_1' - t_2 \geq (1 - k_2/k_1)(t_3 - t_2) \,. \tag{C7}$$

If this inequality is satisfied, a polarization $P(\vec{x}, t_e) = \mathfrak{N} p_{01}\langle \rho_{01}' \rangle + \text{c.c.}$, given by

$$P(\vec{x}, t_e) = -i(\mathfrak{N}/32) p_{01}\theta_3\theta_1'\theta_2|\theta_1|^2 \times e^{i(\vec{k}_1' \cdot \vec{x} - \Omega_{10} t)} e^{-\Gamma_{20}(t_3 - t_1')} + \text{c.c.} \tag{C8}$$

radiates an echo (a SF-II echo) at $t = t_e$. This echo, unlike the SF-I echo, is a fifth-order effect.

As pulses 1 and 1′ merge into a single pulse coincident with pulse 2, the above description ceases to be rigorous. However, we may expect that

an echo will still be emitted at $t_e = t_3$ if (C7) holds, where $t_1' - t_2$ now stands for the time Δt between the center of pulse 2 and the end of pulse 1. For our 5-nsec wide experimental pulses we estimate $\Delta t \simeq 5$ nsec. For the Na $3\,^2S_{1/2}$-$3\,^2P_{1/2}$-$5\,^2S_{1/2}$ three-level scheme, $k_2/k_1 = 0.96$. Thus we may expect an echo if $t_3 - t_2 \leq 125$ nsec, a condition which was always satisfied in our experiments involving this type of echo.

A feature of the SF-II echo which is important for our Na $3\,^2S_{1/2}$-$5\,^2S_{1/2}$ relaxation measurements is the fact that according to (C8) (with $t_e = t_3$) the echo intensity decays as $\exp[-2\eta_{20} p(t_3 - t_1)]$ with increasing foreign-gas pressure p. This allows us to determine η_{20} for the 3*S*-5*S* superposition state.

When pulses 1 and 1′ merge and are simultaneous with pulse 2, the SF-II echo arises as follows: each temporal element of pulse 1 partially transforms the atomic superposition ρ_{21} created by all *previous* elements of pulses 1 and 2 into a superposition ρ_{20} of states 0 and 2. Therefore any rigorous calculation of the SF-II echo for the merged-pulse case of interest must take into account (a) the effect of pulse 1 to at least third order [as is evident from (C8)] and (b) dephasing of the 0-1 superposition *during* pulses 1 and 2. Such a calculation may be done analytically, but the algebra is tedious. We postpone a rigorous derivation until a future publication.

We have observed the following qualitative features of the SF-II echo when observed on the 3*S*-$3P_{1/2}$-5*S* three-level system: (i) the echo intensity decreases at least as fast as the square of the intensity of pulse 1, (ii) within ±2 nsec the echo is simultaneous with pulse 3, (iii) in the absence of foreign gas the SF-II echo decay as a function of t_3 is significantly faster than the rate expected on the basis of the spontaneous radiative decay of the levels involved. All three of these features are predicted by our model of the SF-II echo.

---

*Present address: Avco Everett Research Corp., Everett, Mass., 02149.

[1]C. Füchtbauer and P. Schulz, Z. Phys. 97, 699 (1935). The correction made by Alekseev and Sobel'man (Ref. 8 below) in their analysis of the data of Füchtbauer and Schulz appears to be unwarranted. They base their correction on a reference by A. Ünsold [Vierteljahrsschr. Astronom. Ges. Leipzig 78, 213 (1943)] to a private communication with Füchtbauer. This communication, however, refers to the linewidth cited by Reinsberg [Z. Phys. 105, 460 (1937)] which was *not* corrected for self-broadening. The linewidths reported by Füchtbauer and Schulz (on which our Fig. 6 is based) *are* corrected for self-broadening, albeit in a naive way: the correction was based on the assumption that all the higher resonance lines of an alkali metal are self-broadened by the same amount. Since this is unlikely, we believe that Füchtbauer's graphs can only be trusted qualitatively.

[2]C. Füchtbauer and F. Gössler, Z. Phys. 93, 648 (1935).

[3]C. Füchtbauer and W. von Hessen, Z. Phys. 113, 323 (1939).

[4]For a review of the subject of line broadening see, for example, S. Y. Chen and M. Takeo, Rev. Mod. Phys. 29, 20 (1957).

[5]M. A. Mazing and N. A. Vrublevskaya, Zh. Eksp. Teor. Fiz. 50, 343 (1966) [Sov. Phys. JETP 23, 228 (1966)].

[6]I. I. Sobel'man, *Introduction to the Theory of Atomic Spectra*, (Pergamon, New York, 1972).

[7]C. Reinsberg, Z. Phys. 105, 460 (1937).

[8]V. A. Alekseev and I. I. Sobel'man, Zh. Eksp. Teor Fiz. 49, 1274 (1965) [Sov. Phys. JETP 22, 882 (1966)]. V. A. Alekseev, M. A. Mazing, P. D. Serapinas, I. I. Sobel'man, and L. A. Vainshtein, Proceedings of the Vth ICPEAC, Leningrad, 1967, p. 528.

[9]A. Omont, J. Phys. (Paris) 38, 1343 (1977).

[10]L. S. Vasilenko, V. P. Chebotaev, and A. V. Shishaev, Sov. Phys. JETP Lett. 12, 113 (1970).

[11]G. Grynberg and B. Cagnac, Rep. Prog. Phys. 40, 79 (1977), and references therein.

[12]F. Biraben, B. Cagnac, E. Giacobino, and G. Grynberg, J. Phys. B 10, 2369 (1977).

[13]P. F. Liao, N. P. Economou, and R. R. Freeman, Phys. Rev. Lett. 39, 1473 (1977).

[14]A. Flusberg, T. Mossberg, R. Kachru, and S. R. Hartmann, Phys. Rev. Lett. 41, 305 (1978).

[15]T. Mossberg, A. Flusberg, R. Kachru, and S. R. Hartmann, Phys. Rev. Lett. 39, 1523 (1977).

[16]T. F. Gallagher, S. A. Edelstein, and R. M. Hill, Phys. Rev. Lett. 35, 644 (1975); Phys. Rev. A 15, 1945 (1977). See also the calculations of R. E. Olson, Phys. Rev. A 15, 631 (1977).

[17]C. Y. Robert Wu and W. C. Stwalley, Phys. Rev. A 18, 1066 (1978).

[18]P. R. Berman and W. E. Lamb Jr., Phys. Rev. A 2, 2435 (1970).

[19]T. Mossberg, A. Flusberg, R. Kachru, and S. R. Hartmann (unpublished).

[20]I. D. Abella, N. A. Kurnit, and S. R. Hartmann, Phys. Rev. 141, 391 (1966).

[21]A. Flusberg, T. Mossberg, and S. R. Hartmann, Opt. Commun. 24, 207 (1978).

[22]I. Nagata and Y. Kimura, J. Phys. E 6, 1193 (1973).

[23]J. U. White, J. Opt. Soc. Am. 32, 285 (1942).

[24]E. U. Condon and G. H. Shortley, *The Theory of Atomic Spectra*, (Cambridge University, Cambridge, 1967).

[25]F. Gounand, P. R. Fournier, and J. Berlande, Phys. Rev. A 15, 2212 (1977).

[26]A. Messiah, *Quantum Mechanics* (Wiley, New York, 1962), Vol II.